frontiers | Frontiers in Physics

TYPE Original Research
PUBLISHED 17 January 2023
DOI 10.3389/fphy.2022.1075514

OPEN ACCESS

EDITED BY
Eliana Maria Vasquez Osorio,
The University of Manchester,
United Kingdom

REVIEWED BY
Yoichi Watanabe,
University of Minnesota Twin Cities,
United States
Davide Brivio,
Brigham and Women's Hospital, Harvard
Medical School, United States

*CORRESPONDENCE
Julian Roers,
julian.roers@uni-muenster.de

SPECIALTY SECTION
This article was submitted to Medical
Physics and Imaging,
a section of the journal
Frontiers in Physics

RECEIVED 20 October 2022
ACCEPTED 30 December 2022
PUBLISHED 17 January 2023

CITATION
Roers J, Czarnecki D, Alissa M and Zink K
(2023), Spectral analysis of Monte Carlo
calculated fluence correction and cema
conversion factors for high-energy photon
beams at different depths.
Front. Phys. 10:1075514.
doi: 10.3389/fphy.2022.1075514

Spectral analysis of Monte Carlo calculated fluence correction and cema conversion factors for high-energy photon beams at different depths

Julian Roers[1,2]*, Damian Czarnecki[1], Mohamad Alissa[1] and Klemens Zink[1,3,4]

[1]Institute of Medical Physics and Radiation Protection (IMPS), University of Applied Sciences Giessen, Giessen, Germany, [2]Department of Radiotherapy, University Hospital Münster, Münster, Germany, [3]Department for Radiotherapy and Radiooncology, University Medical Center Giessen-Marburg, Marburg, Germany, [4]Marburg Iontherapy Center (MIT), Marburg, Germany

Purpose: The aim of this study is to investigate the depth-dependent detector response of detailed thimble air-filled ionization chambers by calculating spectral charged particle fluence correction factors at different depths in water. Those spectral correction factors will help to understand, how the detector response varies at different depths and what kind of influences disparate effects have on the spectral detector response.

Methods: The cema-approach can be used to obtain spectral charged particle fluence-based correction factors for various measurement conditions by substituting the commonly well-known dose conversion factor with a conversion factor based on the dosimetric quantity cema ("converted-energy per unit mass"). The resulting spectral fluence correction factors were calculated with the EGSnrc software toolkit and analyzed for two air-filled cylindrical ionization chambers (PTW type 31021 Semiflex 3D, SNC125c™) at different depths in a water phantom irradiated with a 6 MV linear accelerator x-ray spectrum. The ionization chamber models have been stepwise decomposed to investigate the perturbation caused by internal and external effects on the fluence distribution within the detector.

Results: Monte Carlo calculated fluence-based perturbation correction factors revealed that for all investigated detectors, considerable fluence disturbances occur, especially in the build-up region of depth-dose curves. Our results have shown that even slight variations in depth can have major consequences on the differential charged particle fluence within the ionization chamber, mainly due to internal cavity-specific effects. Furthermore, the results showed that in the case of relative dose measurements, the depth-depending detector response can significantly differ from unity in a range of 1.4%–2.8% depending on the ionization chamber design.

Conclusion: The complexity of different effects on the fluence disturbance could be broken down with regard to their influence on the spectral fluence distribution in the sensitive volume of the investigated detectors. It could be demonstrated, that the displacement of water is a depth-depending effect, which can not be compensated or corrected ideally for each investigated water depth by the shift of the effective point of measurement. Generally, the spectral analysis of those energy-dependent

correction factors serves to a deeper understanding of the detector response under various conditions.

KEYWORDS

radiation dosimetry, CEMA, charged particle fluence, detector response, perturbation factor, build-up region, Monte Carlo simulation

1 Introduction

In clinical routine, the absorbed dose to water is commonly obtained from measurements made with an air-filled ionization chamber placed at the point of interest in water. The procedure is based on standards of absorbed dose to water and is specified in current national and international dosimetry protocols such as the IAEA TRS-398 Code of Practice [1]. If the ionization chamber is used under non-calibration conditions, the detector reading has to be corrected using a correction factor obtained theoretically by the fundamental Spencer-Attix cavity theory [2] with the track-end correction by Nahum [3]. This theory is based on the assumption that the presence of an air-filled cavity does not perturb the charged particle fluence spectrum. However, different detector components and cavity-specific influences affect the charged particle fluence. Thus further correction factors are necessary to take into account all deviations from the ideal assumptions made in the Spencer-Attix cavity theory. Such fluence-based correction factors are of considerable interest because the sum of all these factors describes the radiation response of the ionization chamber under various conditions in a proper way.

Monte Carlo (MC) simulation offers a method to obtain the required beam quality correction factor at a given radiation beam quality by calculating the well-known dose conversion factor expressed by the ratio between the absorbed dose to water and the dose determined in the sensitive volume of the ionization chamber. The determination of the dose conversion factor is a straightforward procedure, recommended by Codes of Practice and dosimetry protocols, e.g., the IAEA TRS 398 [1], TG-51 [4, 5] or DIN 6800-2 [6]. Alternatively, the fluence disturbance can be investigated directly by calculating the spectral charged particle fluence under different conditions *via* MC simulations. These fluence spectra can be used to approximate the dosimetric quantity dose by the quantity cema ("converted-energy per unit mass"), which was defined in ICRU Report 60 [7] and revised in ICRU Report 90 [8] as the mean energy lost in electronic interactions in the mass *dm* of a material by secondary charged particles. The cema refers to the fluence distribution of primary charged particles as well as to secondaries of high energies and is thus especially useful for high-energy photon beams [9]. This approximation provides the possibility to substitute the dose conversion factor with a cema conversion factor as introduced by Hartmann et al. [10] in a comprehensive manner which also complies with the fundamental Spencer-Attix cavity formalism. Because the cema can be expressed in terms of the charged particle fluence distribution Φ_E, this approach offers the benefit to decompose the cema conversion factor into a product of energy-dependent (i.e., spectral) fluence-based correction factors $p_{E,i}$ and to analyze the differential fluence spectra with regard to the detector-induced fluence disturbance. Additionally, the cema-approach offers a well-understandable relationship between the spectral fluence disturbance and the resulting detector response. It was suggested by Bouchard [11] and Hartmann et al. [12] that a full account for the detector properties by decomposing detector-specific perturbation correction factors is necessary to determine absorbed dose at different conditions. To follow this suggestion, the global fluence correction factor can be divided into sub-components accounting for the spectral fluence perturbation due to internal cavity-specific effects and external fluence perturbations caused by different detector components [13–15]. In the past years, the MC simulation has become the state-of-art process for the determination of correction factors as described above [16, 17]. In analogy to the dose conversion factor, the cema-approach can also be used to calculate fluence correction factors under non-reference conditions. Hence, correction factors for any changes in the beam quality due to different field size, off-axis distance, or depth can be expressed using the ratio between the cema conversion factors at reference and non-reference conditions.

According to DIN 6800-2 [6] a depth-dependent detector response for photon beams is usually not taken into account so that the non-reference correction factor depends only on the Spencer-Attix restricted stopping power ratios $s^{SA}_{w,med}$. It could be demonstrated that $s^{SA}_{w,med}$ varies by less than 0.3% depending on depth in water [6, 17]. Pena et al. [18] investigated dose conversion factors at shallow depth for a 0.6 cm^3 Farmer type ionization chamber and observed deviations from unity in a range of 12.5% at 0.5 cm depth. Wulff et al. [18] already calculated dose-conversion factors for several ionization chambers under different conditions and concluded that in the build-up region higher correction factors might be necessary depending on the placement of the ionization chamber and its detector components and geometries. There is still limited knowledge regarding the spectral charged particle fluence variations and their effects on the total perturbation correction factors. Nevertheless, those differential correction factors might lead to a closer understanding of spectral fluence changes caused by the detector and the influence of different physical effects on the fluence disturbance in the build-up region. Decomposing these spectral fluence correction factors into several sub-factors providing the perturbation caused by specific detector components can help to understand where the induced fluence changes come from and how the spectral detector response is changing depending on their structural design. More detailed knowledge about these influences might also be helpful to design new detector types with reduced fluence perturbations resulting in a less disturbed spectral fluence response.

This study aims to investigate the depth-dependent detector response of detailed thimble air-filled ionization chambers by calculating spectral fluence correction factors at different depths in water. To better comprehend the role of different cavity-induced and external effects influencing the charged particle fluence spectrum in water, the spectral fluence correction factors are additionally decomposed individually by using decomposition methods introduced by Wang and Rogers [19, 20] and Wulff et al. [15].

With their help, it was also investigated if the positioning of the effective point of measurement as recommended in several dosimetry protocols can adequately compensate for the displacement of water at the build-up region. The purpose of this paper is not primarily the determination of exact correction factors for clinical use, it is more motivated by previous studies that dealt with the general understanding of the detector response under non-equilibrium conditions [10, 12, 18].

2 Materials and methods

2.1 Fundamental dosimetric quantities

The fundamental dosimetric quantities were defined in detail in ICRU Report 60 [7] and were continually corrected in ICRU Report 85 [21] and Report 90 [8]. Concerning the dosimetric quantity absorbed dose, it is usually derived from the energy loss along a given particle track length and is directly related to the dosimetric quantity particle fluence Φ. The absorbed dose to a medium D_{med} due to charged particles can thus be calculated by integrating all differential fluences $\Phi_{E,\mathrm{med}}$ in a medium med of a given particle type multiplied with the associated electronic collision stopping power L as defined in ICRU 85 [22].

$$D_{\mathrm{med}} \overset{\delta-CPE}{=} C_{\mathrm{med}} = \int \Phi_{E,\mathrm{med}} \left[\frac{L}{\rho}\right]_{\mathrm{med}} \mathrm{d}E \tag{1}$$

If there is no delta-particle equilibrium (δ-CPE) the quantity determined is not necessary the absorbed dose but the medium cema C_{med} according to ICRU Report 60 [7, 17]. Because the cema is defined for all charged particles; such as electrons, positrons, protons, etc., the energy transfer per unit distance has to be specified for the existing particle type. In this study, the secondary electron and positron fluence were considered for the calculation of cema, but note that positrons and electrons are not always explicitly separated by word. In ICRU 90 [8] a modified concept; the restricted or reduced cema $C_{\Delta,\mathrm{med}}$ with the correction of track-end terms is defined as:

$$C_{\Delta,\mathrm{med}} = \int_{\Delta} \Phi_{E,\mathrm{med}} \left[\frac{L_\Delta}{\rho}\right]_{\mathrm{med}} \mathrm{d}E + \left\{\Phi_{E,\mathrm{med}}(\Delta)\left[\frac{L(\Delta)}{\rho}\right]_{\mathrm{med}}\Delta\right\} \tag{2}$$

Formally, L_Δ from Eq. 1 has to be replaced by the reduced collision stopping power Λ_Δ as described by Kellerer et al. [9]. Nevertheless, the restricted stopping power as an approach for the reduced collision stopping power offers a good approximation for the applied photon energies and materials used in this study [9, 10]. The restricted medium cema is especially interesting because the requirement that δ-CPE exists can be neglected (Eq. (1)). In regards to MC-applications, the quantity restricted medium cema is also particularly useful, because MC-calculated fluence distributions are derived on a discrete energy grid and also limited by the low-energy cut-off value Δ. Electrons with kinetic energies less than Δ were presented by the so-called track-end term $\mathrm{TE}_{\mathrm{med}} = \Phi_{E,\mathrm{med}}(\Delta)[L(\Delta)/\rho]_{\mathrm{med}}\Delta$ which accounts for local energy depositions.

2.2 Definition of cema conversion factor

According to Hartmann et. al. [10], the cema conversion factor f_{cema} is defined in analogy to the dose conversion factor f_{dose} as the ratio between the restricted water cema at the point of interest $C_{\Delta,\mathrm{w}}$ and the volume-averaged mean restricted medium cema $\bar{C}^{\mathrm{det}}_{\Delta,\mathrm{med}}$ in the cavity (-medium) of the detector:

$$f_{\mathrm{cema}} = \frac{C_{\Delta,\mathrm{w}}}{\bar{C}^{\mathrm{det}}_{\Delta,\mathrm{med}}} \tag{3}$$

with

$$C_{\Delta,\mathrm{w}} = \int_{\Delta}^{E_{\max}} \Phi_{E,\mathrm{w}} \left[\frac{L_\Delta}{\rho}\right]_{\mathrm{w}} \mathrm{d}E + \mathrm{TE}_{\mathrm{w}}$$

and

$$\bar{C}^{\mathrm{det}}_{\Delta,\mathrm{med}} = \int_{\Delta}^{E_{\max}} \bar{\Phi}^{\mathrm{det}}_{E,\mathrm{med}} \left[\frac{L_\Delta}{\rho}\right]_{\mathrm{med}} \mathrm{d}E + \mathrm{TE}^{\mathrm{det}}_{\mathrm{med}}$$

where $\bar{\Phi}^{\mathrm{det}}_{E,\mathrm{med}}$ denotes the spectral charged particle fluence averaged over the cavity volume filled with the medium "med" within the detector and $\Phi_{E,\mathrm{w}}$ is the spectral charged particle fluence in water at the point of interest. Note that the first subscript after Δ from $\bar{C}^{\mathrm{det}}_{\Delta,\mathrm{med}}$ denotes for the medium of the stopping power, i.e. the detector medium. The superscript refers to the surrounding medium. In case the surrounding medium consists of all detector components, a superscript "det" is utilized. If a bare volume is used instead, the superscript is denoted as "w". If the surrounding medium is identical to the medium, in which the fluence is scored, the superscript can be omitted.

For the decomposition of the cema conversion factor f_{cema}, it is necessary to combine a stopping power medium with a different fluence medium, resulting in a hybrid version of restricted cema. Therefore a third subscript is used, which refers to the medium in which the fluence is calculated. If the fluence medium is identical to the stopping power medium, both subscripts are summarized into one subscript. The cema conversion factor f_{cema} can thus be decomposed into a product of sub-factors:

$$f_{\mathrm{cema}} = \frac{C_{\Delta,\mathrm{w}}}{C_{\Delta,\mathrm{med,w}}} \cdot \frac{C_{\Delta,\mathrm{med,w}}}{\bar{C}^{\mathrm{det}}_{\Delta,\mathrm{med}}} = s^{\mathrm{SA}}_{\mathrm{w,med}} \cdot \frac{C_{\Delta,\mathrm{med,w}}}{\bar{C}^{\mathrm{det}}_{\Delta,\mathrm{med}}} \tag{4}$$

where $C_{\Delta,\mathrm{med,w}}$ is the restricted medium cema in water at the point of interest surrounded by water:

$$C_{\Delta,\mathrm{med,w}} = \int_{\Delta}^{E_{\max}} \Phi_{E,\mathrm{w}} \left[\frac{L_\Delta}{\rho}\right]_{\mathrm{med}} \mathrm{d}E + \mathrm{TE}_{\mathrm{med,w}}$$

The first term of Eq. (4) is the Spencer-Attix restricted stopping power ratio water to the cavity medium $s^{\mathrm{SA}}_{\mathrm{w,med}}$. The second term can be denoted as the global fluence correction factor p_{glf} that includes all detector-specific changes of the spectral fluence in relation to the undisturbed spectral fluence in water:

$$p_{\mathrm{glf}} = \frac{C_{\Delta,\mathrm{med,w}}}{\bar{C}^{\mathrm{det}}_{\Delta,\mathrm{med}}} = \frac{\int_{\Delta}^{E_{\max}} \Phi_{E,\mathrm{w}} \mathrm{d}E + \Phi_{E,\mathrm{w}}(\Delta)}{\int_{\Delta}^{E_{\max}} \bar{\Phi}^{\mathrm{det}}_{E,\mathrm{med}} \mathrm{d}E + \bar{\Phi}^{\mathrm{det}}_{E,\mathrm{med}}(\Delta)} \tag{5}$$

The global fluence correction factor can further be decomposed into

$$p_{\mathrm{glf}} = \frac{C_{\Delta,\mathrm{med,w}}}{\bar{C}^{\mathrm{w}}_{\Delta,\mathrm{med}}} \cdot \frac{\bar{C}^{\mathrm{w}}_{\Delta,\mathrm{med}}}{\bar{C}^{\mathrm{det}}_{\Delta,\mathrm{med}}} \tag{6}$$

with the internal fluence correction factor p_{int}

$$p_{\mathrm{int}} = \frac{C_{\Delta,\mathrm{med,w}}}{\bar{C}^{\mathrm{w}}_{\Delta,\mathrm{med}}} \tag{7}$$

which corrects for cavity-specific influences only and p_{ext}

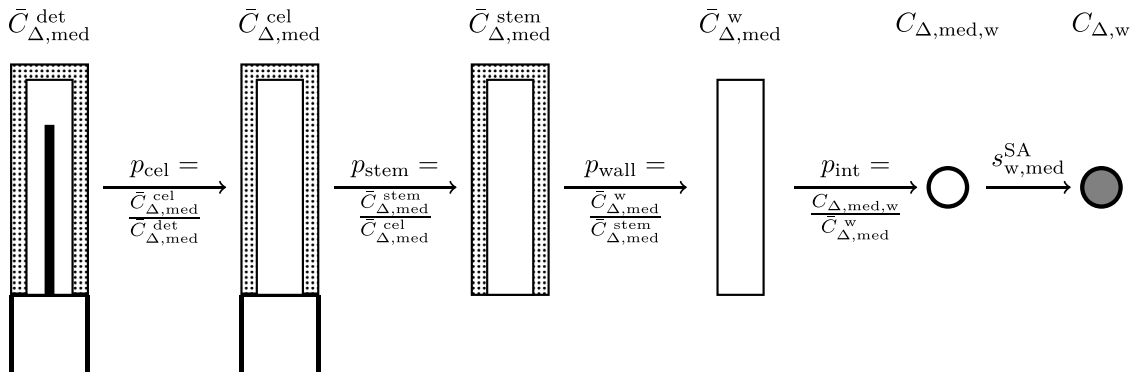

FIGURE 1
Schematic description of the determination of cema-based perturbation factors for air-filled ionization chambers. The principle of this determination method was originally introduced by Wulff et al. [18] and Zink and Wulff [22]. In this study, the fluence correction factors are calculated by comparing the cema values in the cavity while specific constructive details are missing. The internal fluence correction factor p_{int} includes the correction factors for the volume-averaging effect p_{vol}, the density effect p_{ρ} and the displacement effect p_{dis}. The last step describes the conversion between the cema in the air voxel and the cema in a water voxel, which can be described by the Spencer-Attix restricted stopping-power ratio water to the detector medium $s^{\mathrm{SA}}_{\mathrm{w,med}}$.

$$p_{\mathrm{ext}} = \frac{\bar{C}^{\mathrm{w}}_{\Delta,\mathrm{med}}}{\bar{C}^{\mathrm{det}}_{\Delta,\mathrm{med}}} \tag{8}$$

for external fluence perturbations due to different detector components. The external fluence correction factor p_{ext} can also be decomposed into the correction factors from specific constructive detector components for example: p_{cel} for the perturbation caused by the central electrode in an ionization chamber, p_{stem} for the perturbation related to the detector stem and p_{wall} for the perturbation due to the wall (Figure 1). To investigate those specific external fluence correction factors, a decomposition technique introduced by Wulff et al. [18] and Zink and Wulff [22] can be applied. Note that this approach was originally developed for the calculation of dose conversion factors derived from dose ratios. In this study, the restricted cema ratios, respectively the fluence ratios were used. A schematic description of the decomposition technique is shown in Figure 1: The specific fluence correction factors are derived by calculating the cema in the sensitive volume of the ionization chamber while specific components are being removed. In the first step, the volume-averaged restricted medium cema in the detector cavity is calculated while all constructive components are being considered ($\bar{C}^{\mathrm{det}}_{\Delta,\mathrm{med}}$). The second simulation is performed without the central electrode to determine the volume-averaged restricted medium cema in the sensitive detector volume surrounded by all detector components except the central electrode $\bar{C}^{\mathrm{cel}}_{\Delta,\mathrm{med}}$. The fluence correction factor p_{cel} can be calculated subsequently through the ratio of $\bar{C}^{\mathrm{cel}}_{\Delta,\mathrm{med}}/\bar{C}^{\mathrm{med}}_{\Delta,\mathrm{med}}$ and accounts for the fluence perturbation caused by the central electrode. The chain of decomposition can be continued by stepwise removing other detector components and comparing the resulting cema values.

The internal fluence correction factor can be further decomposed into a product of fluence correction factors $p_{\mathrm{int}} = p_{\mathrm{dis}} \cdot p_{\mathrm{vol}} \cdot p_{\rho}$, where p_{dis} corrects the effects due to the displacement of water, p_{vol} corrects the volume-averaging effect and p_{ρ} accounts for the perturbation due to the different physical density of medium "med" in comparison to water (Figure 2). If a measurement is performed with a shift of the effective point of measurement (EPOM), it can be assumed that p_{dis} is equal one [6]. Note that the fluence correction factor p_{fl} accounting for

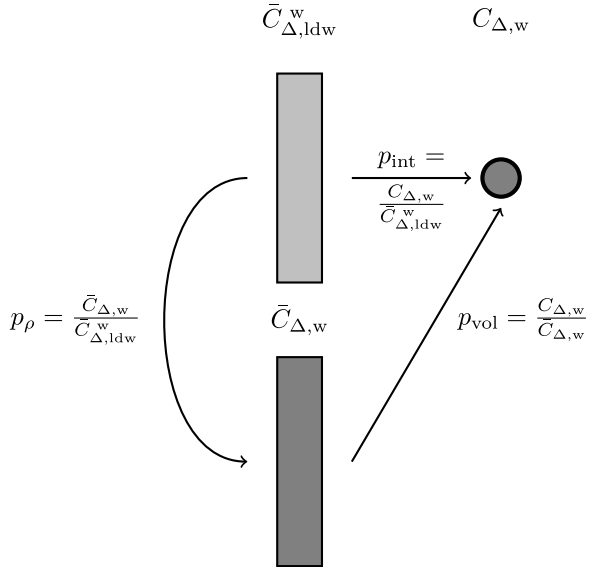

FIGURE 2
Schematic description of the determination of cema-based internal fluence correction factors for air-filled ionization chambers following [19, 20]. The internal fluence correction factor p_{int} includes the volume-averaging effect p_{vol} and the density effect p_{ρ}. The acronym ldw refers to the virtual medium "low-density water". Note that $\bar{C}_{\Delta,\mathrm{w}}$ is determined without the shift of the EPOM [6].

the influence of different atomic compositions on the charged particle fluence was not separately determined in this study [13]. To analyze the spectral behavior of the internal fluence correction factor p_{int} and its sub-factors p_{vol} and p_{ρ} under charged particle dis-equilibrium, a determination method by Wang and Rogers [19, 20] was used. Therefore, a simulation in a cylindrical volume with a length of 0.48 cm and different radii, placed with their shifted reference point at 0.5 cm and 1.5 cm depth in the water phantom, was performed. The first simulation contains a volume filled with "low-density water" (ldw), a virtual material with a physical density of air

and a restricted stopping power of water. The second simulation was performed with a water-filled cavity. The spectral density correction factor p_ρ is thus given as the ratio between the calculated cema values from both simulations. A schematic description of the determination of internal fluence correction factors is shown in Figure 2. It should be pointed out that almost all simulations with a sensitive medium different than liquid water were performed with a shift of EPOM $0.5 \cdot r_{cav}$ away from the focus, where r_{cav} is the internal radius of the chamber cavity, to compensate the influence of the displacement effect according to the DIN6800-2 [6]. In the case of the ldw-filled cylindrical volume as shown in Figure 2, the spectral fluence was once calculated with and once without the shift of EPOM to investigate its influence on the spectral fluence correction factors.

The decomposition in external and internal effects as described above is very similar to Bouchard's decomposition following a sequence of detector components. This formulation is consistent with the classical cavity theory-based factorization of the dose conversion $f_{\text{dose}} = D^{\text{det}}_{\text{med}}/D_{\text{w}}$ for ionization chambers following [1].

$$\frac{1}{f_{\text{dose}}} = f_{\text{cema}} = s^{\text{SA}}_{\text{w,med}} \cdot \prod_i p_i \tag{9}$$

A major advantage of the cema formulation is that all named correction factors can be expressed as a function of energy $p_{E,i}$. For example

$$p_{E,\text{glf}} \coloneqq \frac{\Phi_{E,\text{w}}}{\bar{\Phi}^{\text{det}}_{E,\text{med}}} \tag{10}$$

the energy-independent value of p_{glf} can thus be calculated through the fluence-weighted mean-value of $p_{E,\text{glf}}$, i.e.,

$$p_{\text{glf}} = \frac{\int_\Delta^{E_{\max}} p_{E,\text{glf}} \cdot \bar{\Phi}^{\text{det}}_{E,\text{med}} \mathrm{d}E + \{p_{E,\text{glf}}(\Delta) \cdot \bar{\Phi}^{\text{det}}_{E,\text{med}}(\Delta)\}}{\int_\Delta^{E_{\max}} \bar{\Phi}^{\text{det}}_{E,\text{med}} \mathrm{d}E + \bar{\Phi}^{\text{det}}_{E,\text{med}}(\Delta)} \tag{11}$$

2.3 The non-reference correction factor expressed by cema conversion factors

Under non-reference conditions the determined dose has to be corrected by the conceptual foundation included in the current DIN 6800-2 dosimetry protocol [6]. The factor k_{NR} corrects any changes of the beam-quality correction factor k_{Q} due to different field size FS, off-axis distance R, depth z or source-to-surface distance SSD compared to the geometrical reference conditions with

$$k_{\text{NR}} = \frac{k_{\text{Q}}(z, \text{FS}, \text{R}, \text{SSD})}{k_{\text{Q}}(10\,\text{cm}, 10\,\text{cm} \times 10\,\text{cm}, 0\,\text{cm}, 100\,\text{cm})} \tag{12}$$

and can also be expressed by

$$k_{\text{NR}} = \frac{(D_{\text{w}}/D_{\text{med}})_{\text{NR}}}{(D_{\text{w}}/D_{\text{med}})_R}. \tag{13}$$

Analogously to the dose conversion factor $D_{\text{w}}/D_{\text{med}}$, a cema conversion factor $C_{\text{w}}/C_{\text{med}}$, introduced by Hartmann et al. [10] can be used to calculate the non-reference correction factor k_{NR}:

$$k_{\text{NR}} \overset{\delta\text{-}CPE}{=} \frac{(C_{\text{w}}/C_{\text{med}})_{\text{NR}}}{(C_{\text{w}}/C_{\text{med}})_R} \tag{14}$$

In this study, k_{NR} is calculated as a function of depth z.

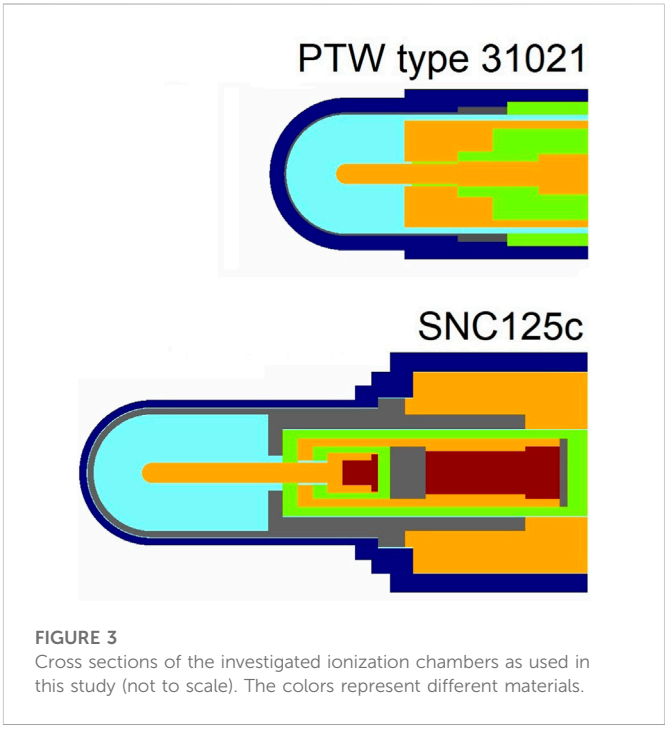

FIGURE 3
Cross sections of the investigated ionization chambers as used in this study (not to scale). The colors represent different materials.

2.4 Monte Carlo simulation setup

The simulations were performed with a modified version of the EGSnrc user code egs_chamber [22]. The charged particle fluence scoring was adopted from the user code cavity [23] and extended using the track-end correction method III as described in [24]. A short overview of the fluence calculation method is given in [10, 24]. The choice of the Monte Carlo user code egs_chamber is motivated by high usability for dosimetric calculations of air-filled ionization chambers. In a previous study [25] and internal work reports the compatibility of all used variance-reduction techniques was confirmed. With the modified user code, the absorbed dose D, the spectral electron as well as the positron fluence $\bar{\Phi}_E$ were calculated for two thimble air-filled ionization chambers (PTW type 31021 Semiflex 3D and Sun Nuclear SNC125c™). Details on selected detector properties and cross sections of the used MC-models can be found on the manufacturer's websites and in Figure 3. All quantities were also calculated for a small cubic water voxel of 1 mm side-length. The restricted spectral cema $C_{\Delta,E}$ was calculated using Eq. (2). Following the formalism introduced by Hartmann et al. [10], the global fluence correction factor $p_{E,\text{glf}}$ (Eq. (5)), the cema conversion factor $f_{E,\text{cema}}$ (Eq. 4) and its sub-factors $p_{i,E}$ (as described in Figures 1, 2)- all differential in energy -were derived by the differential charged particle fluence Φ_E and the Spencer-Attix restricted stopping-power ratio $s^{\text{SA}}_{\text{w,a}}$ at different depths in a cubic water phantom with 30 cm side length. Due to the fact that the positron fluence proportion is usually in the order of a few percent of the total charged particle fluence Φ, all shown energy-dependent $p_{E,i}$ in Section 3 are calculated for electrons. The total fluence correction factors were calculated by taking into account the positron fluence according to Eq. (11). All detectors were oriented with their axis perpendicular to the beam axis and placed with their reference point at depth from 0.5 cm to 20 cm, considering the shift of the EPOM according to DIN6800-2 [6]. The phantom was irradiated with a 6 MV linear accelerator x-ray spectrum taken from Mohan [26] from a

TABLE 1 Summary of simulation properties and parameters with EGSnrc, according to the recommendations of AAPM TG-268.

Item	Description	References
Code	EGSnrc code system	Kawrakow [29]
	egs++ class library	Kawrakow et al. [23]
	modified version of `egs_chamber`	Wulff et al. [22]
Validation	Fano cavity test: SNC125c™	Alissa et al. [30]
	PTW type 31021 Semiflex 3D used in previous studies	Tikkanen et al. [31]
Timing	Absorbed dose to medium D_{med}, high resolution spectral fluence Φ_E calculation and the determination of cema C for the following simulations require: Section 3.1: 475 single CPU hours, Section 3.2: 675 single CPU hours, Section 3.3: 5800 single CPU hours (2.1 GHz) on average for each performed simulation	
Source description	6 MV linear accelerator x-ray spectrum taken from Mohan, from a collimated point source with a field size of 10 cm × 10 cm and an SSD of 100 cm	Mohan et al. [26]
Cross sections	XCOM photon cross section	
Transport parameters	Boundary crossing algorithm: Exact; global `ECUT` 512 keV and `PCUT` 1 keV	
Variance reduction techniques	Photon cross-section enhancement (XCSE) with an enhancement factor of 256 and Russian Roulette range rejection technique (RR) with a survival probability of 1/256 and an `ESAVE` value of 512	Wulff et al. [22]
Scored quantities	Absorbed dose to med D_{med}, high resolution spectral fluence Φ_E for electrons and positrons with a binsize of 1 keV and the determination of (fluence-based) cema C	
Statistical uncertainties	$\leqq$ .1% for all absorbed dose; $\leqq$ .1% for all total electron fluence; $\leqq$ 0.2% for all total positron fluence; uncertainties for differential fluence distributions vary with energy	
Statistical method	History-by-history	
Postprocessing	Bin-averaging and calculation of the fluence-weighted mean values of fluence correction and cema-weighted mean values of cema conversion factors with an application written in R	

collimated point source with a field size of 10 cm × 10 cm and an SSD of 100 cm. The value of the common photon beam quality specifier $TPR_{20,10}$ at a 10 cm × 10 cm field size amounts to 0.671 using the approach Followill et al. [27]. The non-reference correction factors k_{NR} for different depths in water are calculated using Eq. (14).

For all calculations, a low-energy cut-off limit from 1 keV kinetic energy was used. The lower limit of the spectral fluence calculation was also set to 1 keV as well as the energy resolution of the spectral charged particle fluence but all calculated ratios in Figures 5–10 have been averaged over a logarithmic bin size from 1 keV to 100 keV in order to reduce statistical fluctuations. The Russian Roulette (RR) and cross-section enhancement (XCSE) were used to decrease the statistical uncertainties and gain efficiency due to reduced CPU runtimes. The RR-Parameter ESAVE was therefore set to the ECUT-value of 512 keV to produce an accurate spectral fluence distribution. For the RR—and XCSE-Region, the detector was covered with a cylindrical volume with a +1 cm shell thickness filled with water. For depths 0.5 cm and 1 cm the RR- and XCSE-region was extended as far as the surface of the water phantom was reached. The general simulation settings, according to the recommendations of AAPM TG-268 [29] are shown in Table 1.

3 Results

3.1 Depth-depending fluence spectra in water

In Figure 4A the undisturbed electron fluence spectrum $\Phi_{E,w}$ is shown at different depths in water evoked by the irradiation with a 6 MV linear accelerator x-ray spectrum taken from Mohan [26]. For clarity reasons, the spectral electron fluence in 2 cm, 5 cm and 20 cm water depth were omitted in Figure 4. Qualitatively, it can be seen that $\Phi_{E,w}$ is depth-dependent while the highest fluence occurs at a water depth of 1.5 cm. For energies above 4 MeV, the spectral electron fluence decreases by several orders of magnitude and converges to zero. The relative secondary electron fluence at depth z normalized to 1.5 cm water depth given in Figure 4B revealed that $\Phi_{E,w}$ changes differently in energy depending on depth in water: In the build-up region, the relative electron fluence spectrum systematically depends on energy; especially in the high-energy range whereas at 10 cm water depth only slight spectral fluctuations occur.

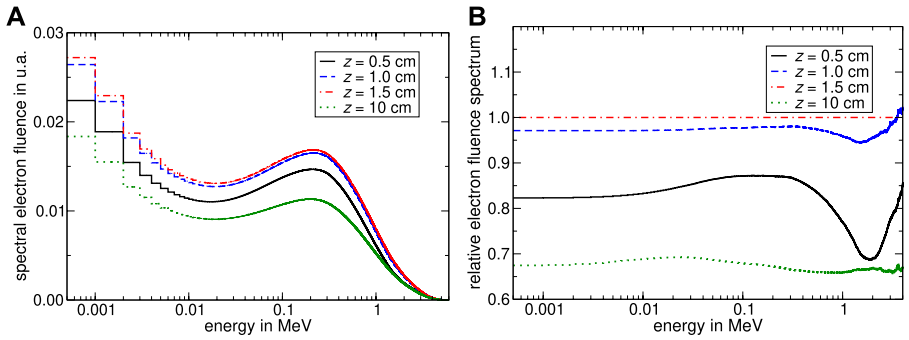

FIGURE 4
Monte Carlo calculated spectral secondary electron fluence in water at different depths. The water phantom was irradiated with a 6 MV linear accelerator x-ray spectrum taken from Mohan [26] from a collimated point source with a field size of 10 cm × 10 cm. Subfigure **(A)** shows the secondary electron fluence as a function of energy. Panel **(B)** shows the relative secondary electron fluence spectrum normalized to the spectral electron fluence at 1.5 cm water depth. The uncertainty varies depending on energy in a range of 0.005%–0.5% for panel **(A)** and 0.01%–1.2% for panel **(B)**.

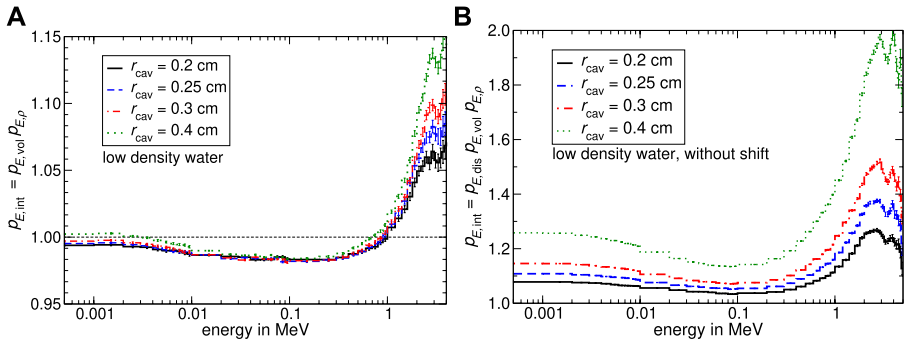

FIGURE 5
Monte Carlo calculated spectral internal fluence correction factors for a cavity with a length of 0.48 cm and different radii filled with "low-density water" as a function of energy at the build-up region. In subfigure **(A)** the cavity was oriented with its axis perpendicular to the beam axis and placed with their reference point shifted by $0.5 \cdot r_{cav}$ away from the focus. In panel **(B)** the spectral internal fluence correction factors are shown, whereby the reference point is placed at 0.5 cm depth. The uncertainty varies depending on energy in a range of 0.05%–1.3% for panel **(A)** and 0.07%–1.9% for panel **(B)**.

3.2 Internal fluence correction factors in the build-up region

In Figure 5 the spectral internal fluence correction factor $p_{E,\mathrm{int}}$ for a "low-density water"-filled cavity of different radii and 0.48 cm length is shown as a function of charged particle energy in 0.5 cm water depth irradiated by a 6 MV linear accelerator x-ray spectrum [26]. Because the positron fluence proportion is $>2\%$ of the total charged particle fluence Φ, all shown energy-dependent $p_{E,i}$ in Section 3 are for electrons. Nevertheless, the positron fluence was included for the calculation of the energy-independent total fluence correction factors p_i as tabled in Table 2 and Table 3. It is important to note that a correction factor p_i smaller than unity indicates that the charged particle fluence in the bare volume $\bar{\Phi}^{w}_{\mathrm{med}}$ is greater compared to the undisturbed water fluence Φ_w. In Figure 5A the spectral internal fluence correction factor is shown for a cavity, whereby the reference point was shifted by $0.5 \cdot r_{cav}$ away from the focus to compensate the influence due to the displacement of water. It can be seen that the internal fluence correction factor $p_{E,\mathrm{int}}$ for the energy spectrum from 0 to 1 MeV is smaller than unity for all cylinder radii (with only one exception for $r = 0.4$ cm, in the spectrum from 0 to 5 keV). For energy values above 1 MeV, the internal fluence correction factor is increasing. The largest deviation of $p_{E,\mathrm{int}}$ from unity can be observed for the cavity with the largest radius.

To verify the influence of the displacement effect in the build-up region, a simulation without the shift of the EPOM was performed. Comparing the spectral internal fluence correction factor $p_{E,\mathrm{int}}$ from Figure 5A, B, indicates that the displacement effect is nearly compensated by the positioning of the cavity $0.5 \cdot r_{cav}$ away from the focus; in particular for energies below 1 MeV. The increase of $p_{E,\mathrm{int}}$ from Figure 5A for energies >1 MeV hence can be seen *inter alia* as an effect of uncompensated displacement. Thus it appears that in the proper meaning the fluence correction factor for the density effect $p_{E,\rho}$ given in Figure 6B and hence the internal fluence correction factor $p_{E,\mathrm{int}}$ shown in Figure 5A includes the correction of displacement too.

According to the procedure shown in Figure 2, the spectral internal fluence correction factor $p_{E,\mathrm{int}}$ from Figure 5A was factorized into the subfactors $p_{E,\mathrm{vol}}$ and $p_{E,\rho}$ (Figure 6). The fluence correction factors for the volume-averaging effect $p_{E,\mathrm{vol}}$ shown in Figure 6A is approximately constant for all energies and varies with the particle's energy likely by 1%–3%. Generally $p_{E,\mathrm{vol}}$

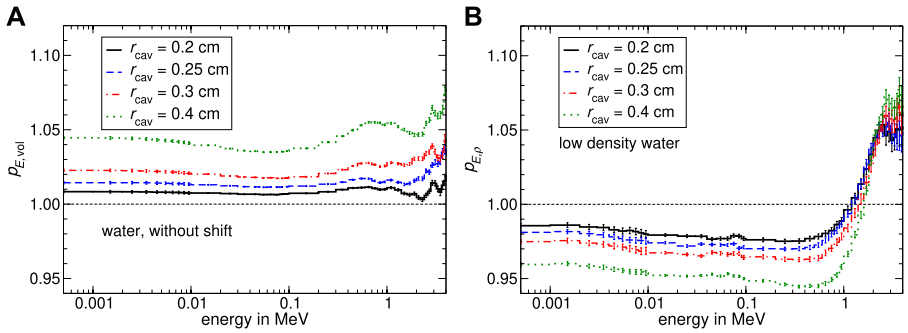

FIGURE 6
Monte Carlo calculated volume-averaging correction factor $p_{E,vol}$ and density correction factor $p_{E,\rho}$ as a function of energy in the build-up region determined by the factorization of the internal fluence correction factor shown in Figure 5A. The spectral volume-averaging correction factor $p_{E,vol}$ is shown in panel **(A)**. In subfigure **(B)** The density effect correction factor $p_{E,\rho}$ as a function of energy was calculated by the quotient of $p_{E,int}$ divided by $p_{E,vol}$ as shown in Figure 2. The uncertainty varies depending on energy in a range of 0.09%–0.5% for panel **(A)** and 0.14%–1.8% for panel **(B)**.

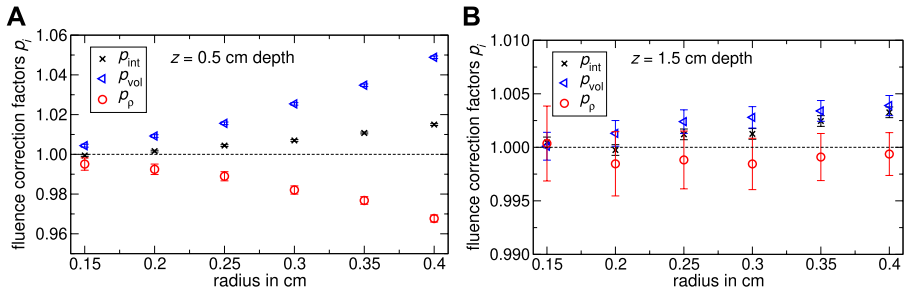

FIGURE 7
The Monte Carlo calculated internal fluence correction factor p_{int}, the volume-averaging correction factor p_{vol} and the density correction factor p_{ρ} for the cavity with a length of 0.48 cm and different radii in **(A)** 0.5 cm and **(B)** 1.5 cm water depth. The uncertainty varies likely by 0.2% for p_{int}, respectively p_{vol} and 0.4% for p_{ρ}.

is greater than unity for all cylinder radii. As shown in Figure 6B the calculated density correction factor $p_{E,\rho}$ is below unity for energies from 0 to 1 MeV and greater than unity for energies >1 MeV for all investigated cylinder radii.

In Figure 7A the Monte Carlo calculated internal fluence correction factors p_{int} as well as the factorization into the subfactors p_{ρ} and p_{vol} are shown as a function of the cavity radius. For a water depth of 0.5 cm a systematic dependency on the cavity radius is observable: on the one hand p_{vol} is increasing with increasing cavity radii. Conversely p_{ρ} is decreasing almost by the same margin as p_{vol} is increasing. For a cavity radius of 0.5 cm both effects have a maximum deviation from unity of below 5‰. The volume-averaging correction factor p_{vol} prevails over the density effect correction factor p_{ρ} for all cavity radii. Consequently the internal fluence correction factor p_{int} is greater unity for all investigated cavity radii. The fluence correction factors for 1.5 cm water depth are shown in Figure 7B. All fluence correction factors differ from unity with a maximum deviation of 0.4%, while p_{vol} is greater; and p_{ρ} is below unity. The volume correction factor p_{vol} is only slightly increasing depending on the cavity radius whereby the internal fluence correction factor is increasing by a few tenths of a percentage too. The density effect correction factor p_{ρ} remains constant within the range of uncertainties.

3.3 Cema conversion and fluence correction factors for air-filled cylindrical ionization chambers at different depths

In Figure 8 the global fluence correction factor $p_{E,glf}$ and the cema conversion factor $f_{E,cema}$ differential in energy at different depths in water are shown for cylindrical ionization chambers irradiated with a 6 MV linear accelerator x-ray spectrum taken from Mohan [26]. A value of $p_{E,glf}$ below unity implements that the particles fluence in the ionization chamber $\bar{\Phi}^{det}_{med}$ is greater compared to the undisturbed fluence in water Φ_w, which corresponds to an over-response of the detector. Concerning the global fluence correction factor $p_{E,glf}$ as shown in Figure 8, a systematic dependency on secondary electron's energy is observable: In the low-energy spectrum at reference conditions the global fluence correction factor $p_{E,glf}$ is increasing until it reaches a maximum at 0.2 MeV. For the PTW type 31021 $p_{E,glf}$ is decreasing for energies above 0.2 MeV, resulting in a relative

TABLE 2 Specific fluence correction factors p_i for the perturbation caused by different constructive details from the PTW 31021 and SNC125c™ as well as the calculated dose-conversion factor according to Eq. 9. The uncertainties vary below 0.1% for all unmarked values.

Detector	Depth z	i	f_{dose}	p_i
PTW 31021	0.5 cm	p_{cel}	0.994	0.995
		p_{stem}	0.986	0.986
		p_{wall}	0.996	0.995
		p_{int}	1.104	0.995
		p_{ext}	0.97 (7)	0.97 (6)
		p_{glf}		0.97 (1)
	10 cm	p_{cel}	0.998	0.998
		p_{stem}	0.997	0.998
		p_{wall}	1.002	1.001
		p_{int}	1.115	1.000
		p_{ext}	0.99 (7)	0.99 (7)
		p_{glf}		0.99 (7)
SNC125c™	0.5 cm	p_{cel}	0.991	0.992
		p_{stem}	0.995	0.995
		p_{wall}	0.992	0.993
		p_{int}	1.114	1.002
		p_{ext}	0.97 (9)	0.98 (0)
		p_{glf}		0.98 (2)
	10 cm	p_{cel}	0.994	0.997
		p_{stem}	1.001	1.001
		p_{wall}	1.002	1.001
		p_{int}	1.118	1.002
		p_{ext}	0.99 (7)	0.99 (9)
		p_{glf}		1.00 (1)

minimum at approximately 1 MeV. Compared to the PTW 31021, the relative minimum is only slightly pronounced for the SNC125c™. For high energies, the spectral global fluence correction factor $p_{E,glf}$ at reference conditions converges to unity. The detector response from ionization chambers is also depending on depth in water: For energies below 2 MeV, the over-response is increasing with decreasing water depth. At 0.5 cm water depth, $p_{E,glf}$ for high energies is increasing resulting in an under-response of the ionization chamber.

As described in Section 2.2, the cema conversion factor $f_{E,cema}$ is calculated by multiplying with the Spencer-Attix restricted stopping-power ratio $s^{SA}_{w,med}$ differential in energy. For air-filled ionization chambers, $f_{E,cema}$ is greater than unity for all energies, whereby it varies in a range of 0.2% in the low-energy spectrum.

In Figure 9A the specific fluence correction factors for constructive details from the PTW type 31021 as a function of energy are shown for a depth of 0.5 cm in water. The fluence correction factor for the perturbation caused by the central electrode $p_{E,cel}$ is quite constant as a function of energy and differs from unity in a range of 2% for high electron energies. The wall perturbation correction factor $p_{E,wall}$ changes marginally by ~1% in the energy range from 0 to 1 MeV and decreases for energies below 1 MeV. On the contrary, the fluence correction factor for the influence of the stem $p_{E,stem}$ is smaller than unity and shows a substantial decrease in the energy spectrum from 0.2 MeV to 1 MeV with a maximum deviation from unity from nearly 3%. As can be seen in Figure 9A, the internal fluence correction factor depends on energy and follows the course of $p_{E,int}$ shown in Figure 6 with only one exception: An decrease occur in the low-energy spectrum.

Concerning the spectral specific fluence correction factors $p_{E,i}$ at 10 cm water depth as shown in Figure 9B, the wall and central electrode correction factors stay nearly constant as a function of energy compared to 0.5 cm water depth. The energy-independent total correction factors are differing from their values at 0.5 cm water depth by only 0.8%. The deviation from unity from the stem correction factor is decreasing, resulting in a fluence-weighted mean-value of p_{stem} with an amount of 0.998 while the decrease in the energy spectrum from 0.2 MeV to 1 MeV is less noticeable. The spectral internal fluence correction factor $p_{E,int}$ for a water depth of 10 cm converges to unity with increasing energy, leading to a total p_{int} of ~1.

The spectral specific fluence correction factors for the perturbation caused by constructive details from the SNC125c™ are shown in Figure 10. Especially in the case of the fluence disturbance due to the detector stem, spectral differences between the Semiflex 3D and the SNC125c™ are observable: While the stem perturbation correction factor $p_{E,stem}$ for the PTW 31021 depends on the energy, it is approximately constant as a function of energy for the SNC125c™. On the contrary, the spectral fluence perturbation caused by the wall and the central electrode looks quite similar. All resulting specific fluence correction factors p_i are shown in Table 2. Note that the internal correction factor p_{int} based on the dose conversion factors includes the Spencer-Attix restricted stopping power ratio water to air $s^{SA}_{w,air}$ whereas it is excluded in the fluence-based approach on the right-hand side.

All calculated values for cylindrical air-filled ionization chambers are summarized in Table 3. Note that p_{glf} is numerically equal to p_Q. The k_Q value for the PTW 31021 was calculated using the cema approximation $k_Q = f_{cema}(TPR = 0.671)/f_{cema}(^{60}Co)$ in 10 cm depth with $f_{cema}(^{60}Co) = 1.127$. The result amounts to 0.986 and agrees within the uncertainty of 0.3% given for the data of the consensus k_Q values for MV photon beams updated in the IAEA TRS-398 [32].

In Table 3 the calculated p_{glf} and k_{NR} (see Eq. (14)) for air-filled cylindrical ionization chambers are shown as a function of depth. The global fluence correction factor p_{glf} for the PTW 31021 varies within a range of 3%, the non-reference correction factor increases depending on the chamber type roughly by the same percentage. In comparison, the SNC125c™ have a slighter influence on the undisturbed charged particle fluence Φ_w in water at 0.5 cm depth, whereas it changes only by an amount of < 2%. The resulting non-reference correction factor k_{NR} is depth-dependent and changes in the order of ~ 3%.

TABLE 3 Monte Carlo calculated fluence correction, cema - as well as dose conversion factors for cylindrical air-filled ionization chambers as a function of depth in water irradiated with a 6 MV linear accelerator x-ray spectrum taken from [26] from a collimated point source with a field-size of 10 cm × 10 cm. The uncertainties vary below 0.1% for all calculated values.

Detector	Depth z in cm	f_{dose}	f_{cema}	$s^{SA}_{w,med}$	p_{glf}	k_{NR}
PTW 31021	0.5	0.927	1.078	1.111	0.970	0.969
	1.0	0.910	1.101	1.114	0.988	0.990
	1.5	0.904	1.108	1.115	0.994	0.997
	2.0	0.902	1.110	1.115	0.996	0.999
	5.0	0.901	1.111	1.114	0.996	0.999
	10.0	0.901	1.112	1.115	0.997	1.000
	20.0	0.902	1.110	1.114	0.996	0.999
SNC125c™	0.5	0.917	1.091	1.111	0.982	0.978
	1.0	0.904	1.106	1.113	0.994	0.992
	1.5	0.899	1.112	1.113	0.999	0.997
	2.0	0.898	1.114	1.114	1.000	0.998
	5.0	0.897	1.115	1.115	1.000	0.999
	10.0	0.896	1.116	1.115	1.001	1.000
	20.0	0.897	1.114	1.114	1.000	0.999

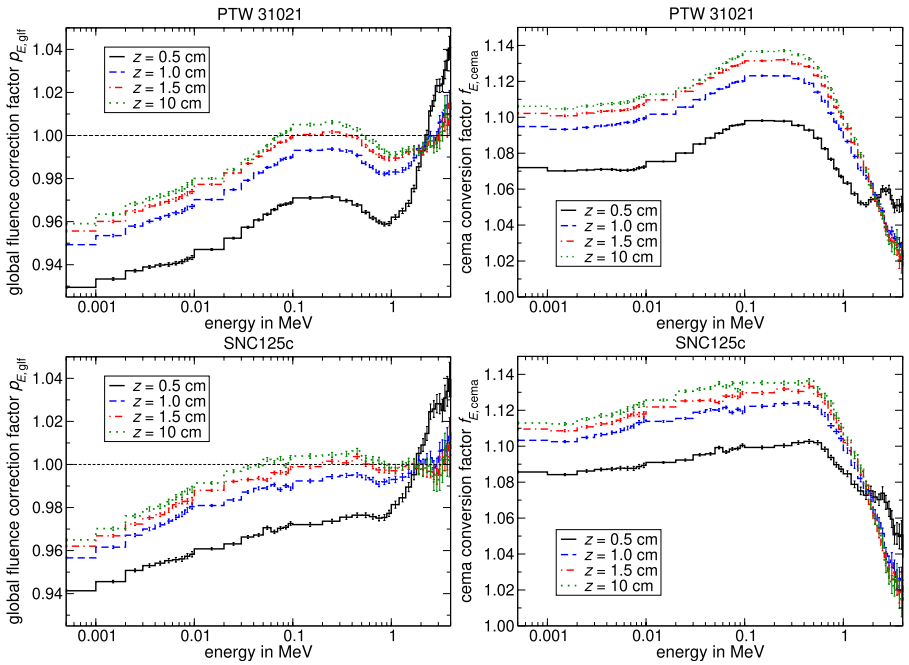

FIGURE 8
Monte Carlo calculated global fluence correction factors $p_{E,glf}$ and cema conversion factors $f_{E,cema} = p_{E,glf} \cdot s^{SA}_{w,med}$ differential in energy for cylindrical air-filled ionization chambers placed with their shifted reference point at different depths in water. The uncertainty varies depending on energy in a range of 0.05%–1%.

In the following, it can be summarized that considerable changes in the spectral electron fluence in water occur in the low-energy spectrum due to the presence of the investigated detectors, especially in the build-up region. According to Eq. (2), the restricted medium cema $C_{\Delta,med}$ is calculated by integrating the spectral electron and positron fluence in the medium Φ_{med} weighted by the associated restricted stopping powers $L_{\Delta,med}$. Hence disturbances in the spectral electron fluence particularly in the lower energy range are more meaningful with respect to the determined cema.

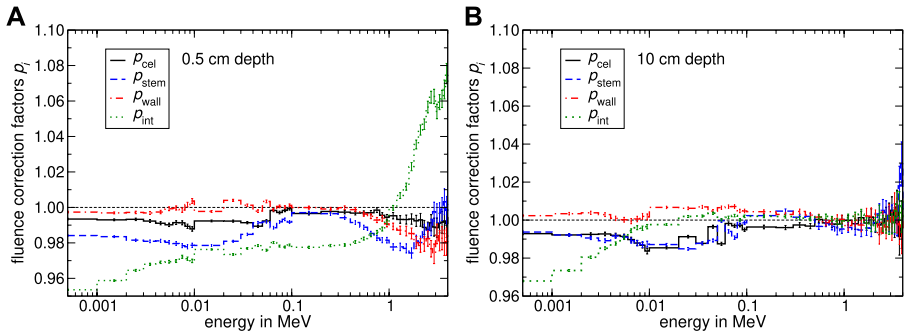

FIGURE 9
Monte Carlo calculated specific fluence correction factors $p_{E,i}$ for different constructive details from the PTW 31021 Semiflex 3D as a function of energy. Panel **(A)** shows the spectral specific fluence correction factors $p_{E,i}$, whereby the shifted EPOM was positioned at 0.5 cm depth. In subfigure **(B)** $p_{E,i}$ was calculated at 10 cm depth. The uncertainty varies depending on energy in a range of 0.05%–1%.

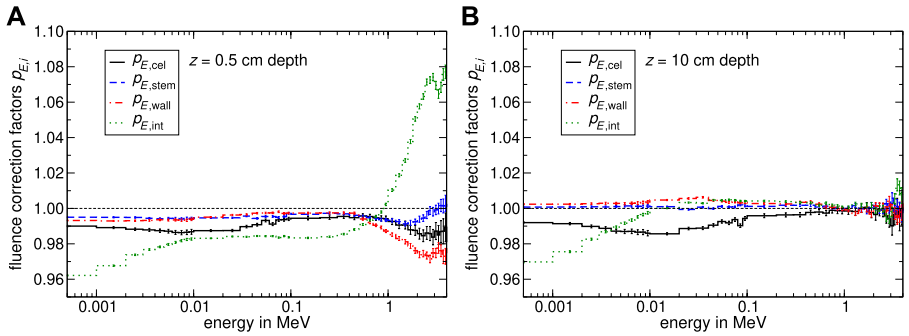

FIGURE 10
Monte Carlo calculated specific fluence correction factors $p_{E,i}$ for different constructive details from the SNC125c™ as a function of energy. Panel **(A)** shows the spectral specific fluence correction factors $p_{E,i}$, whereby the shifted EPOM was positioned at 0.5 cm depth. In subfigure **(B)** $p_{E,i}$ was calculated at 10 cm depth. The uncertainty varies depending on energy in a range of 0.06%–0.9%.

4 Discussion

4.1 Influence of the internal fluence correction factor in the build-up region

Our results have shown that even small changes in depth can have major effects on the differential charged particle fluence in the ionization chamber in the build-up region, mainly due to internal effects. The internal fluence correction factor can be further reduced to the product of the density effect $p_{E,\rho}$ and the volume-averaging effect $p_{E,\mathrm{vol}}$. It could also be shown that the displacement effect of water is nearly compensated by the positioning of the chamber $0.5 \cdot r_{\mathrm{cav}}$ away from the focus.

In the build-up region, the volume-averaging effect $p_{E,\mathrm{vol}}$ is leading to a constant lower electron fluence $\bar{\Phi}_{E,\mathrm{w}}$ in the cavity compared to the fluence $\Phi_{E,\mathrm{w}}$ in water for all energies especially with increasing cavity radii. On the contrary, the lower density of air compared to water is leading to an over-response in the fluence spectrum below 1 MeV. This over-response might be explained by the lateral scattering of secondary particles in the cavity and the significantly greater range of charged particles in air compared to water. For high electron energies, an under-response occurs, which might be explained by (1) the depth-depending variations in the electron spectrum in water (Figure 4) in combination with (2) the partially uncompensated displacement effect.

1. As shown in Figure 3, distinctive fewer electrons in water exist in the energy range above 0.5 MeV in the build-up region compared to the spectrum at 1.5 cm water depth. The interpretation of the resulting leak of high-energy electrons is not so intuitive but might be explained in a qualitative manner by the energy-dependent existence of charged particle equilibrium (CPE): Per definition, CPE exists for a volume if each charged particle of a given type and energy leaving the cavity is replaced by an identical particle with the same physical properties [2]. Thus CPE can only be achieved at a depth z equal or greater compared to the linear continuous slowing-down range R_{CSDA} of the electron with energy E. The existence of CPE hence in fact depends on the kinetic energy E of secondary charged particles and the given medium. Considering a water-filled cavity the fluence distribution consists of electrons that are getting created inside the cavity (“starters”) and those entering the cavity from outside (“crossers”) [12]. If the bare volume is filled with air, the charged particle fluence is merely due to particles entering the cavity from outside and crossing it completely (Bragg-Gray condition). The increased CSDA-range R_{CSDA} due to the

finite size of the air-filled cavity and the assumption that no electrons are created inside might lead to a lower fluence in the high-energy spectrum in the air-filled cavity compared to the water-filled one.

2. The shift of the EPOM for cylindrical ionization chambers accounts for the displacement of the surrounding medium by the finite size of the detector. It could be defined as the point in water where the incoming particle fluence spectrum in the sensitive volume of the air-filled cavity $\bar{\Phi}^{w}_{E,air}$ is comparable to the fluence in the idealized Bragg-Gray detector, respectively the undisturbed fluence spectrum in water $\Phi_{E,w}$ so that no displacement correction factor p_{dis} is required. As can be seen in Figure 5A, this requirement is only partially satisfied in the build-up region, especially in the high-energy range of the fluence spectrum. Nevertheless, the shift of EPOM is leading to considerably fewer spectral discrepancies between $\Phi_{E,w}$ and $\bar{\Phi}^{w}_{E,air}$ (compare Figure 5). Additionally, the total fluence correction factor is obtained by calculating the fluence-weighted mean value of the spectral fluence correction factors according to Eq. (11). Hence, the spectral variations of $p_{E,int}$ in the high-energy electron fluence spectrum only accounts for a small impact on the determined total internal fluence correction factor p_{int}.

Next to this effect, the depth-dependent secondary charged particle fluence spectrum is leading to variations in the restricted stopping power ratios $s^{SA}_{w,air}$ from ~ 0.3% like already demonstrated by [6, 18].

4.2 Spectral analysis of the global fluence correction and cema conversion factors for air-filled ionization chambers

The internal fluence correction factor as discussed in Section 4.1 was calculated for a volume with approximately similar dimensions compared to the size of the sensitive volume from the PTW type 31021 Semiflex 3D. It is therefore possible to compare the course of both internal fluence correction factors as a function of energy at 0.5 cm water depth (compare $p_{E,int}$ for r_{cav} = 0.25 cm shown in Figure 5A with $p_{E,int}$ from Figure 9A). If the volume is filled with air (Figure 9A), $p_{E,int}$ increases in the energy range up to 100 keV. As can be seen in Figure 5A, where the volume was filled with low-density water the increase of the internal fluence correction factor is neglected and $p_{E,int}$ is approximately constant. The only difference between both simulations is that the stopping-powers (on the one hand $L_{\Delta,w}$ and on the other hand $L_{\Delta,air}$) differ from each other due to diverse electron densities n ($\propto Z/A$) and mean excitation potentials I ($\propto Z$) of the used media. Concerning the physical density and the size of the volume, they were quasi identical. Bouchard et al. [13] pointed out that various atomic compositions of the detector medium will cause the energy absorption to differ due to differences in the interaction cross-sections. This effect primarily influences the fluence of low-energy charged particles and was denoted by Bouchard as p_{fl}. The influence of different stopping-powers and atomic compositions (i.e., p_{fl}) on the fluence calculation might be a possible explanation for the increase of $p_{E,int}$ from Figure 9A. However, the conclusions about concerning $p_{E,int}$ from Section 4.1 can also be applied to air-filled ionization chambers.

With increasing complexity of the simulation geometry, it becomes difficult to derive a specific effect due to the superimposition of several influencing factors on the spectral charged particle fluence. As described in Figure 1 the decomposition into specific external effects can help to analyze the perturbation caused by different detector components on the spectral fluence in the detector. As shown in Figure 8 the spectral global fluence correction factor $p_{E,glf}$ is smaller than unity in the energy range from 0 to 100 keV leading to an over-response in the low-energy fluence spectrum. Figure 9, 10 showed that the presence of the central electrode is resulting in a constant higher secondary charged particle fluence in the detector cavity $\bar{\Phi}^{det}_{E,air}$ in comparison to the undisturbed water fluence $\Phi_{E,w}$. The over-response in the low-energy fluence spectrum is also enhanced by the production of secondary charged particles in the wall and especially in the stem. In the medium energy range from 100 keV to 2 MeV a decrease of the global fluence correction factor $p_{E,glf}$ occurs, which can be assigned to the production of medium energy electrons due to the stem and the scattering of those into the sensitive volume. Also the fluence correction factors $p_{E,cel}$ and $p_{E,wall}$ are decreasing in the build-up region, whereby they remained constant within the range of uncertainties at 10 cm water depth. Interestingly, the fluence perturbation caused by the stem seems to be smaller for the SNC125c™ compared to the PTW type 31021 Semiflex 3D. The smaller length of the sensitive volume from the Semiflex 3D in comparison to the SNC125c™ might be the reason for the higher influence of the stem on the charged particle fluence distribution in the PTW type 31021 Semiflex 3D. In the high-energy spectrum with energies greater than 2 MeV, the global fluence correction factor in the build-up region is mainly affected by the described internal effects mentioned in Section 4.1. At 10 cm depth, $p_{E,int}$ for electron energies greater than 0.6 MeV is nearly constant for both investigated ionization chambers and differs from unity by only 0.2%.

Concerning the resulting total stem correction factor p_{stem} for the PTW type 31021 calculated in this study, it is 0.998 at 10 cm which is in good agreement with findings from Wulff et al. [15, 18] for the PTW type 31010 Semiflex. Furthermore, the relatively high proportion of aluminum in the PTW 31021 stem model in comparison to the idealized stem used by Wulff et al. [15, 18] seems to have no influence on the total stem correction factor at all. At 0.5 cm depth, the stem correction factor p_{stem} showed an amount of 0.987 and is next to the internal fluence correction factor one of the main reasons for the significantly pronounced over-response in the build-up region. The total fluence correction factor for the central electrode at 0.5 cm depth is in good agreement with simulated values from Wulff et al. [15]. In addition, the total fluence correction factor for the influence of the chamber wall on the charged particle fluence was found to be 0.2% larger.

4.3 Non-reference correction factor k_{NR} at different depths and its influence on relative measurements

Multiple studies have been investigating the influence of non-reference conditions especially in the case of small fields [33–35]. A changed detector response for the determination of depth-dose curves or relative distributions for photon beams with ionization chambers is usually not taken into account and the correction factor k_{NR} is assumed to be unity. There are also several studies [36, 37] that reported differences in the detector response in the build-up region

depending on the choice of the EPOM. The study of Pena et al. [36] assumed that if a measurement of a percentage depth-dose curve is performed without a shift of EPOM, further depth-dependent conversion factors should be used accounting for the variations in the depth-dependent detector response. Wegener et al. [37] could reduce the influence of different detector responses on relative measurements by using detector-individually derived effective points of measurement.

This study showed that the non-reference correction factor k_{NR} is depth-depending and varies likely by 3% for the Semiflex 3D and 2% for the SNC125c™ due to different values of the specific fluence correction factors p_i from constructive details and due to the depth-depending variations in the Spencer-Attix restricted stopping power ratios in an order of approximately 0.3% (Table 3). Mainly, the spectral differences in the build-up region are due to the energy-dependent dis-equilibrium and the involved steep gradients which are responsible for the variations in the detector response under non-equilibrium conditions. Under equilibrium conditions in depths behind the dose maximum, k_{NR} for air-filled ionization chambers varies likely by 0.2% with increasing water depth. Concerning the non-reference correction factors k_{NR} for air-filled ionization chambers found in this study displayed good agreement with findings from Wulff et al. [15]. In further studies, the existence of δ-CPE in the build-up region and thus the validity of Eq. (14) should be investigated.

The results of this study have shown that in high-energy photon beams, the shift of EPOM is always a compromise solution and does not offer an ideal correction for all depths at the build-up region. Due to the non-linear depth-dependency of p_{glf} or k_{NR} shown in Table 3, it could make sense to determine the absorbed dose to water at the build-up region without the shift of EPOM and use instead detector-individually derived depth-dependent correction factors as described by Pena et al. [36]. Those depth-dependent correction factors can be obtained for individual depths and beam qualities *via* Monte Carlo simulations.

5 Conclusion

The cema-formalism provides the possibility to determine energy-dependent (spectral) fluence-based correction factors accounting for the detector-induced charged particle fluence disturbance and to analyze the detector response as a function of energy. In this study, spectral cema- and fluence-based correction factors for two ionization chambers were calculated with a modified version of the Monte Carlo user code egs_chamber. The step-by-step decomposition of spectral fluence-based correction factors made it possible to consider sub-factors separately from the superimposition of several influencing effects. The spectral analysis of fluence correction factors in the build-up region offered that the spectral detector response of air-filled ionization chambers is strongly affected by the depth-dependent variations in the charged particle fluence spectrum in water due to the absence of CPE. Whereas the external effects change marginally, the influence of cavity-induced effects is considerably increasing with decreasing depth. Additionally, a systematic dependency on the secondary particle's energy could be observed for the density and displacement effect. Furthermore, a compensation of the displacement effect can not fully be achieved by the shift of the effective point of measurement $0.5 \cdot r_{cav}$ away from the focus.

Additionally, it was shown that the total fluence correction factor for a specific effect p_i as tabulated in several dosimetry protocols can deviate considerably from the energy-dependent perturbation factor $p_{E,i}$ accounting for the same effect. It should be noticed that the total fluence correction factor p_i accounts for the mean-spectral fluence disturbance weighted by the spectral fluence distribution in the detector's sensitive volume. The characteristic fluence distribution is responsible for the fact that fluence disturbances in the low-energy spectrum are more influential regarding the resultant total perturbation factor p_i than perturbations in the high-energy range. Accordingly, effects like the partially uncompensated displacement of water, which mainly affects the high-energy spectral fluence, only contribute to a small impact on the determined global fluence correction factor. Nevertheless, it should be attempted to keep the spectral fluence disturbance as low as possible no matter in which energy range of spectrum. Therefore it is necessary to further investigate the influence of different detector geometries and components on the spectral electron and positron fluence distribution in the future.

Data availability statement

The original contributions presented in the study are included in the article/Supplementary Material, further inquiries can be directed to the corresponding author.

Author contributions

The authors confirm their contribution to the paper as follows: study conception and design: JR, DC, and KZ; data collection: JR and MA; analysis and interpretation of results: JR, DC, and KZ; draft manuscript preparation: JR and DC. All authors reviewed the results and approved the final version of the manuscript.

Conflict of interest

The authors declare that the research was conducted in the absence of any commercial or financial relationships that could be construed as a potential conflict of interest.

Publisher's note

References

1. IAEA. Absorbed dose determination in external beam radiotherapy: An international code of Practice for dosimetry based on standards of absorbed dose to water. No. 398 in Technical Reports Series. Vienna: International Atomic Energy Agency (2001). updated 2006 v.12).

2. Spencer LV, Attix FH. A theory of cavity ionization. *Radiat Res* (1955) 3:239–54. doi:10.2307/3570326

3. Nahum AE. Water/air mass stopping power ratios for megavoltage photon and electron beams. *Phys Med Biol* (1978) 23:002–38. doi:10.1088/0031-9155/23/1/002

4. Almond PR, Biggs PJ, Coursey BM, Hanson WF, Huq MS, Nath R, et al. AAPM's TG-51 protocol for clinical reference dosimetry of high-energy photon and electron beams. *Med Phys* (1999) 26:1847–70. doi:10.1118/1.598691

5. McEwen M, DeWerd L, Ibbott G, Followill D, Rogers DW, Seltzer S, et al. Addendum to the AAPM's TG-51 protocol for clinical reference dosimetry of high-energy photon beams. *Med Phys* (2014) 41:041501. doi:10.1118/1.4866223

6. DIN6800-2. Procedures of dosimetry with probe-type detectors for photon and electron radiation - Part 2: Ionization chamber dosimetry of high energy photon and electron radiation. Technical report (Normenausschuß Radiologie (NAR) im DIN) (2020).

7. ICRU. Fundamental quantities and units for ionizing radiation. ICRU Report 60. Bethesda: International Commission on Radiation Units and Measurements (1998). 13–7. doi:10.1093/jicru/os31.1.13

8. ICRU. Key data for ionizing radiation dosimetry: Measurement standards and applications. ICRU Report 90. Bethesda: International Commission on Radiation Units (2016).

9. Kellerer AM, Hahn K, Rossi HH. Intermediate dosimetric quantities. *Radiat Res* (1992) 130:15–25. doi:10.2307/3578474

10. Hartmann GH, Andreo P, Kapsch R-P, Zink K. Cema-based formalism for the determination of absorbed dose for high-energy photon beams. *Med Phys* (2021) 48: 7461–75. doi:10.1002/mp.15266

11. Bouchard H, Kamio Y, Palmans H, Seuntjens J, Duane S. Detector dose response in megavoltage small photon beams. II. Pencil beam perturbation effects. *Med Phys* (2015) 42:6048–61. doi:10.1118/1.4930798

12. Hartmann GH, Zink K. Decomposition of the dose conversion factor based on fluence spectra of secondary charged particles: Application to lateral dose profiles in photon fields. *Med Phys* (2018) 45:4246–56. doi:10.1002/mp.13081

13. Bouchard H, Seuntjens J, Carrier J-F, Kawrakow I. Ionization chamber gradient effects in nonstandard beam configurations. *Med Phys* (2009) 36:4654–63. doi:10.1118/1.3213518

14. Buckley L, Rogers DWO. Wall correction factors, Pwall, for thimble ionization chambers. *Med Phys* (2006) 33:455–64. doi:10.1118/1.2161403

15. Wulff J, Heverhagen J, Karle H, Zink K. Investigation of correction factors for non-reference conditions in ion chamber photon dosimetry with Monte-Carlo simulations. *Z medizinische Physik* (2010) 20:25–33. doi:10.1016/j.zemedi.2009.09.003

16. Borg J, Kawrakow I, Rogers DWO, Seuntjens JP. Monte Carlo study of correction factors for Spencer-Attix cavity theory at photon energies at or above 100 keV. *Med Phys* (2000) 27:1804–13. doi:10.1118/1.1287054

17. Andreo P. Monte Carlo simulations in radiotherapy dosimetry. *Radiat Oncol (London, England)* (2018) 13:121. doi:10.1186/s13014-018-1065-3

18. Wulff J, Heverhagen J, Zink K. Monte-Carlo-based perturbation and beam quality correction factors for thimble ionization chambers in high-energy photon beams. *Phys Med Biol* (2008) 53:2823–36. doi:10.1088/0031-9155/53/11/005

19. Wang LL, Rogers DWO. Calculation of the replacement correction factors for ion chambers in megavoltage beams by Monte Carlo simulation. *Med Phys* (2008) 35:1747–55. doi:10.1118/1.2898139

20. Wang LL, Rogers DWO. Replacement correction factors for cylindrical ion chambers in electron beams. *Med Phys* (2009) 36:4600–8. doi:10.1118/1.3213094

21. ICRU. Fundamental quantities and units for ionizing radiation (revised), ICRU report 85b*International Commission on Radiation Units. Bethesda* (2011) 2011:23–8. doi:10.1093/rpd/ncs077

22. Wulff J, Zink K, Kawrakow I. Efficiency improvements for ion chamber calculations in high energy photon beams. *Med Phys* (2008) 35:1328–36. doi:10.1118/1.2874554

23. Kawrakow I, Mainegra-Hing E, Rogers DWO, Tessier F, Walters BRB. *The EGSnrc C++ class library NRCC Report PIRS-898*. Ontario, Canada: National Research Council of Canada (2020).

24. Hartmann GH, Andreo P. Fluence calculation methods in Monte Carlo dosimetry simulations. *Z für Medizinische Physik* (2019) 29:239–48. doi:10.1016/j.zemedi.2018.08.003

25. Failing T, Hartmann G, Hensley F, Keil B, Zink K. Enhancement of the egsnrc code egs_chamber for fast fluence calculations of charged particles. *Z für Medizinische Physik* (2022) 32:417–27. doi:10.1016/j.zemedi.2022.04.003

26. Mohan R, Chui C, Lidofsky L. Energy and angular distributions of photons from medical linear accelerators. *Med Phys* (1985) 12:592–7. doi:10.1118/1.595680

27. Followill DS, Tailor RC, Tello VM, Hanson WF. An empirical relationship for determining photon beam quality in TG-21 from a ratio of percent depth doses. *Med Phys* (1998) 25:1202–5. doi:10.1118/1.598396

28. Rogers DWO, Bazalova-Carter M, Bolch WE, Heath EC, McNitt-Gray MF, Sempau J, et al. Records: Improved reporting of Monte Carlo RaDiation transport studies: Report of the AAPM research committee task group 268. *Med Phys* (2018) 45:e1–5. doi:10.1002/mp.12702

29. Kawrakow I. The EGSnrc Code System, Monte Carlo Simulation of electron and photon transport. NRCC Report PIRS-701 (2017).

30. Alissa M, Zink K, Tessier F, Schoenfeld A, Czarnecki D. Monte Carlo calculated beam quality correction factors for two cylindrical ionization chambers in photon beams. *Physica Med* (2022) 94:17–23. doi:10.1016/j.ejmp.2021.12.012

31. Tikkanen J, Zink K, Pimpinella M, Teles P, Borbinha J, Ojala J, et al. Calculated beam quality correction factors for ionization chambers in MV photon beams. *Phys Med Biol* (2020) 65:075003. doi:10.1088/1361-6560/ab7107

32. Andreo P, Burns DT, Kapsch R-P, Zink K, Vatnitsky S, Andersen CE, et al. Determination of consensus k_Q values for megavoltage photon beams for the update of IAEA TRS-398. *Phys Med Biol* (2020) 65:095011. doi:10.1088/1361-6560/ab807b

33. Alfonso R, Andreo P, Capote R, HuqSaiful M, Kilby W, Kjäll P, et al. A new formalism for reference dosimetry of small and nonstandard fields. *Med Phys* (2008) 35: 5179–86. doi:10.1118/1.3005481

34. Bouchard H, Seuntjens J, Duane S, Kamio Y, Palmans H. Detector dose response in megavoltage small photon beams. I. Theoretical concepts. *Med Phys* (2015) 42:6033–47. doi:10.1118/1.4930053

35. Kumar S, Fenwick JD, Underwood TS, Deshpande DD, Scott AJ, Nahum AE. Breakdown of Bragg–Gray behaviour for low-density detectors under electronic disequilibrium conditions in small megavoltage photon fields. *Phys Med Biol* (2015) 60:8187–212. doi:10.1088/0031-9155/60/20/8187

36. Pena J, Sánchez-Doblado F, Capote R, Terrón JA, Gómez F. Monte Carlo correction factors for a Farmer 0.6 cm^3 ion chamber dose measurement in the build-up region of the 6 MV clinical beam. *Phys Med Biol* (2006) 51:1523–32. doi:10.1088/0031-9155/51/6/011

37. Wegener S, Herzog B, Sauer OA. Detector response in the buildup region of small MV fields. *Med Phys* (2020) 47:1327–39. doi:10.1002/mp.13973